The Skipper CCD for low-energy threshold particle experiments above ground

Guillermo Fernandez Moroni,[1] Fernando Chierchie,[2] Javier Tiffenberg,[1] Ana Botti,[3] Mariano Cababie,[3,1] Gustavo Cancelo,[1] Eliana L. Depaoli,[4] Juan Estrada,[1] Stephen E. Holland,[5] Dario Rodrigues,[3,1] Iván Sidelnik,[6] Miguel Sofo Haro,[1,7] Leandro Stefanazzi,[1] and Sho Uemura[8]

[1]*Fermi National Accelerator Laboratory, PO Box 500, Batavia IL, 60510, USA.*
[2]*Instituto de Inv. en Ing. Eléctrica "Alfredo Desages" (IIIE),*
Dpto. de Ing. Eléctrica y de Computadoras. CONICET and
Universidad Nacional del Sur (UNS), Bahía Blanca, Argentina.
[3]*Department of Physics, FCEN, University of Buenos Aires and IFIBA, CONICET, Buenos Aires, Argentina.*
[4]*CNEA - Gerencia de Área Aplicaciones de la Tecnología Nuclear (GAATN) - Gerencia Química Nuclear y Ciencias de la Salud - Dpto. Metrologia de Radioisotopos - Division Metrologia Científica Centro Atómico Ezeiza.*
[5]*Lawrence Berkeley National Laboratory, One Cyclotron Road, Berkeley, California 94720, USA.*
[6]*CONICET y CNEA - Comisión Nacional de Energía Atómica, Departamento de física de neutrones,*
Centro Atómico Bariloche, Av. Bustillo 9500, Bariloche, Argentina.
[7]*Centro Atómico Bariloche, CNEA/CONICET/IB, Bariloche, Argentina.*
[8]*School of Physics and Astronomy, Tel-Aviv University, Tel-Aviv 69978, Israel.*
(Dated: August 31, 2021)

We present experimental results using a single-electron resolution Skipper-CCD running above ground level to demonstrate the potential of this technology for its use in reactor neutrino observations and other low-energy particle interaction experiments. Operating conditions and event-selection criteria are provided to decouple most of the background rate at low energies. Our final results for events with energies as low as 5 ionized electron-hole pairs show that the exponentially increasing rate of events seen in other technologies is not present in our data. This demonstrates that the Skipper CCD proves to be among the best options to measure low energy and weakly interacting particles at ground level.

I. THICK FULLY DEPLETED CCDS FOR PARTICLE DETECTION EXPERIMENTS

Charged Coupled Devices (CCD) with low readout noise and large active volume have been identified among the most promising detector technologies for the low-mass direct dark-matter search experiments, probing electron and nuclear recoils from sub-GeV mass [1–5]. The recent development of the Skipper-CCD [6–8] demonstrated the capability to measure ionization events with sub-electron noise extending the reach of this technology to unprecedented low energies. This enabled world leading results for dark matter searches at underground facilities [8]. Experiments based on this technology are planned for the coming years with active masses going from 100 grams to several kilograms [9, 10], running at underground facilities that allows to rule out most of the cosmic background. At the same time, the low-noise CCD technology has been implemented in low-energy neutrino experiments [11, 12] above surface; implementing Skipper-CCDs is also planned for future developments [13].

CCD sensors to be used in future instruments are part of a significant R&D effort [9, 10, 13]. One of the most important performance requirement to fully exploit the single counting capability of the Skipper-CCD is the control of the background signals below 1 keV. Rates of single electron depositions larger than expected have been observed in [8], and its possible link to higher-energy particles has been summarized in [14]. Moreover, recent

studies on regions in the CCD with low collection efficiency [15] show how large-energy ionization events could produce low-energy signals in the detector. For this reasons, experiments running above ground are more challenging due to the larger rate of atmospheric high-energy particles [16, 17]. Several new low-threshold technologies observe a rapidly increasing rate of background events towards low energies (below 1 keV). This effect is more evident when detectors are not operated underground. Larger background rates result in limiting the reach of the low-threshold capability. The first edition of the EX-CESS workshop in 2021 [18] exhibit the effort of the community to overcome this issue.

In [19] it is shown that a good control of the background starting at 15 eV up to 500 eV is a key factor for new physics searches using neutrinos at nuclear reactors. Moreover, other studies such as the silicon energy absorption for photons and neutrons scatterings are critical and require Skipper-CCDs running at the surface level with controlled levels of background. It is fairly known that the long readout time of these sensors does not allow the use of active veto systems. For this reason, passive shield configurations together with event selection criteria based on the spatial resolution of thick fully-depleted CCDs are used to reject undesired signals.

In this article we study the use of Skipper-CCDs as a potential low-threshold technology for experiments above surface. We discuss the main sources of background found on the measurements. We propose a detector operation scheme and selection criteria to reject these

contributions. We demonstrate that with the proposed technique, the low energy excess in the background rate seen by other experiments [18] is not present using the Skipper-CCD technology, even down to events producing an ionization of 5 electron-hole pairs (just electrons from now on). Finally, we compare the background measurements observe by other low threshold technologies already published that have participated in the EXCESS workshop.

II. DESCRIPTION OF THE EXPERIMENT

Figure 1 (a) shows the experimental setup where some of the main components are labeled. One Skipper-CCD (shown in Fig. 1 (b)) was operated at a temperature of 140 K using a Sunpower cryocooler [20]. The CCD is glued to a silicon substrate that sits on a Copper tray for mechanical support as well as thermal connectivity. The CCD is placed in an extension of the dewar that fits inside a lead cylinder. A lead cap on top of the sensor (inside the dewar extension) completes the lead shield of two inches of thickness around the device. There was no radio purity selection of materials inside the shield. The CCD was designed by the LBNL Microsystems Laboratory (MSL) [21] and fabricated at Teledyne-DALSA. It has 6144 columns by 1024 rows with pixels of 15 μm by 15 μm with a thickness of 675 μm. It is read by four amplifiers, one on each corner, using a Low Threshold Acquisition (LTA) controller [22]. Two quadrants presented larger readout noise and were not used for the analysis in the following sections. The sensor was operated at sub-electron noise by averaging 300 measurements of the charge in each pixel [7] and with a horizontal binning [23] of 10 columns.

Two different kind of measurements were performed:

- DATA-SET A: Interactions in the active region. 3.21 days of data were collected from the active region of the sensor in continuous readout mode [8].

- DATA-SET B: Interactions collected in the serial register (also called horizontal register). It consists of charge packets collected only by the serial register, not coming from the active region, from here on called "serial-register events"[1]. To make an isolated measurement of this source of events, the vertical lines of the sensor were left in idle mode while clocking only the control signals from the serial and

_____

[1] Later it will be shown that these depositions dominate the low energy spectrum in the output data. This charge is generated in the inactive silicon surrounding the active volume on the edges of the die. The charge can diffuse from the undepleted region and eventually reach the collection region of the pixels in the serial register. For more information about the sensor electrostatic see [24].

output stage. In other words, the sensor is read out as in DATA-SET A but without moving the charge from the active area to the serial register. 2.7 days were collected in this mode.
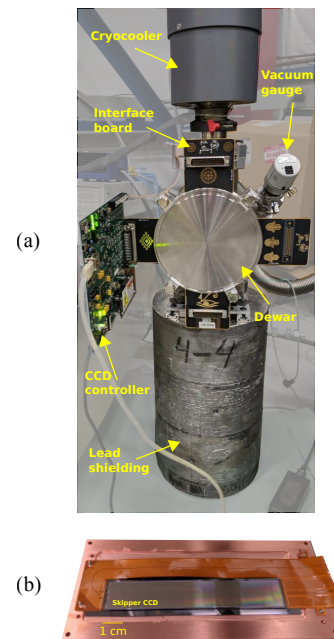

FIG. 1. (a) Setup used for the experiment with a short description of the main components. (b) A picture of the CCD installed on the Copper tray. An extra Copper plate that covers the top part of the sensor is not presented in the image.

III. DETECTOR CALIBRATION AND NOISE SOURCES

An absolute energy calibration of the sensor is performed using the electron counting capability. A histogram of the pixel values from the active region (DATA-SET A) is produced as shown in Fig. 2. Each peak correspond to a discretized number of electrons in the pixel after the calibration and is fitted using a Gaussian distribution whose mean value is used to build a look-up table (digital unit vs. electrons) to calibrate the sensor up to around 700 e^-. To calibrate the sensor at 2146 e^-, single pixel X-ray events with energy of 8.048 keV produced by the fluorescence of the surrounding copper material are also used. We assume an average energy deposition per collected electron of 3.75 eVee [25].

The readout noise of the sensor, evaluated as the standard deviation of the values of the empty pixels (0 e^- peak in Fig. 2), is 0.165 e^- and 0.167 e^- for the two quadrants in use. The average single electron rate per pixel measured are 0.01 e^-/pix and 0.009 e^-/pix after binning in each quadrant, with a contribution from the exposure dependent charge production [26] of 0.018 e^-/pix/day (pixels before binning). The diffusion charge transport

of carriers in the bulk of the sensor was measured and it turned out to be similar to the previously published in [8].
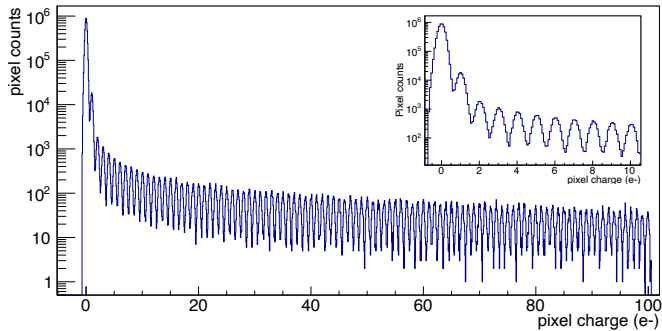

FIG. 2. Histogram of pixels with charge up to $100e^-$ after calibration. Single electron discrimination is observed. The inset shows the same histogram for the first ten peaks.
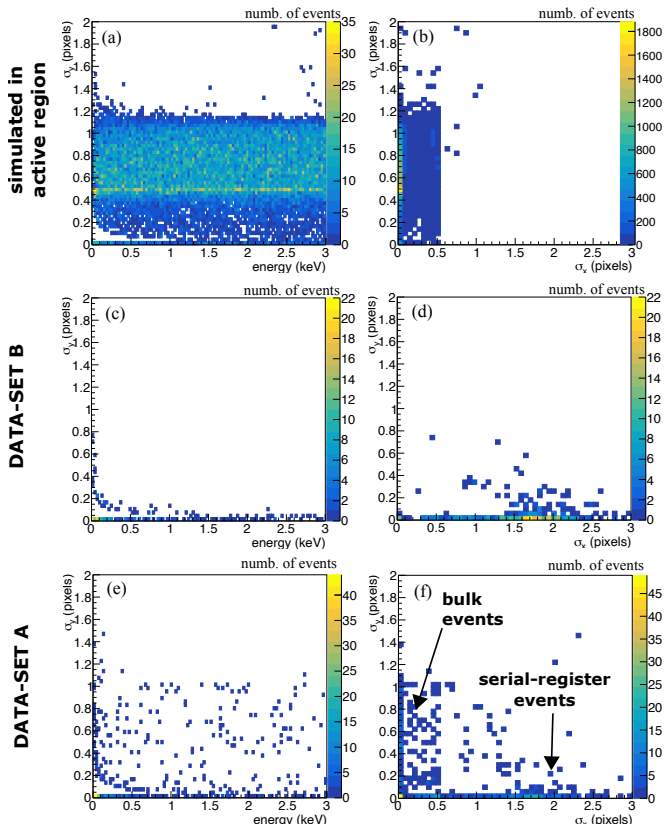
IV. STUDY OF THE EXTRACTED INTERACTION

FIG. 3. Morphology of the events in the output image: (a) and (b) are the expected events from true interactions in the sensor generated from simulations; (c) and (d) serial-register events contributions measured without dumping the collected charge in the active volume to the serial register; and (e) and (f) measured events in the active region of the sensor.

Figure 3 shows the shape and energy distributions of the events analyzed. Left plots show the event size in the y-direction (rows of the image), σ_y (determined as the standard deviation of the charge distribution in the pixels of the event) as a function of energy for three different data sets: the two previously discussed and a third set generated from a simulation. The plots on the right show the relationship between the size (σ_x) in x-direction (columns of the image) and σ_y.

Figure 3(a) and (b) correspond to simulations of particle energy depositions in the active region (bulk) of the sensor. Spatially and energetically uniformly distributed events (30000 events) of charge ionization from 5 to 800 electrons were simulated in the bulk [27] using the charge transport calibration curve in [8]. Since the charge of ten columns is collapsed into one due to the horizontal binning, there is little information left concerning the shape of the event in the x-direction of the output images as shown in Fig. 3 (b). Some events present $\sigma_x > 0$. They take place on the edge of the binned regions and have information shared between two binned pixels and their probability of occurrence is low.

From Fig. 3(a) we can see that the σ_y distribution is similar for all energies. Most of the events have a σ_y larger than 0.4 pixels (see color scale) with a maximum of about 1.1 pixels due to the maximum expected lateral diffusion.

Figure 3(c) and (d) shows the distribution of events measured in the serial register (DATA-SET B). A dark-current signal following a Poisson distribution with mean equal to 0.01 e^-/pixel (after binning, as expected in DATA-SET A) was added to emulate both contributions together. In contrast to the events in the bulk, these ones show a σ_y distribution close to 0. Since the charge is only collected in one row (the serial register), serial-register events have practically no spatial information in the y-direction. They extend on the x-direction projecting on the σ_x axis. Low-energy events may appear with an increased size in the y-direction due to dark counts in neighboring pixels paired in the same cluster.

The third group in Fig 3(e) and (f) corresponds to measurements in the active region of the sensor (DATA-SET A). The plots show components of the previously mentioned contribution: events from the bulk (as in the simulations) and from the serial register. The firsts have sizes below 1.1 pixels in y-direction and smaller than 0.5 pixel in x-direction, as expected from the charge transport calibration and event simulations, while the latter populates both plots for small σ_y.

As shown in the previous analysis, the proposed horizontal binning provides the advantage of orthogonalizing the size information of both sources of events, and therefore a more pure selection of bulk events can be made. It also accelerates the total readout time needed to read the pixel charge while staying in the serial register, and thus it reduces the exposure time to this source of spurious events.

V. EVENT SELECTION, FINAL SPECTRUM AND COMPARISON WITH OTHER TECHNOLOGIES

Figure 4(a) shows the measured differential spectra of events in the active region with 5 or more electrons of ionized charge (from DATA-SET A). Columns of the CCD that presented high single electron rate (hot columns [23]) were eliminated from the analysis at an early stage. The remaining active mass of the sensor in use is 0.675 grams. The gray plot depicts all events reconstructed from the output images showing a monotonic increase of the rate towards low energy. The peak at around 8 keV corresponds to the fluorescence X-rays from the copper in the mechanical package of the sensor. To study the impact of the results obtained in the previous section a selection criteria based on the event shape was performed. Figure 5 shows the one dimensional distribution of the size, in x and y directions, for the events simulated in the active region of the sensor. Although events in the bulk can show a size in σ_x up to 0.5 pixels (Fig. 5(a)), the majority of them (72%) have a width smaller than 0.1 pixels. A constraint of $\sigma_x < 0.3$ is used to provide strong rejection to the serial-register and dark-current events. At the same time, only sizes in the y-direction compatible with depositions in the bulk are selected: $0.3 < \sigma_y < 1$. The minimum limit is to prevent counting serial-register events. The spectrum of events after the selection cuts is also shown in blue in Fig. 4(a). Most of the low energy excess was removed because its contribution was coming from the serial register. The average flux of events with equivalent deposited energy from 5 e^- to 2000 e^- (7.5keV) is 12 kdru. The plot does not show any significant increase of events towards low energies. The spectrum is normalized by the active mass of the sensor, but not by the efficiency of the selection criteria.

To evaluate the efficiency of the selection criteria, simulated events from interactions spatially and energetically uniformly distributed in the active volume of the sensor were added to the real images. The diffusion transport model of carriers were also used in this simulation. The percentage of reconstructed events passing the selection criteria are shown in Fig. 4(b). Each energy bin is 50 eV wide and the first bin starts at 15 eV (equivalent to 5 electrons included). The efficiency is almost flat for all energies showing that the final shape of the spectra is not modified by the selection criteria. The red curve shows a linear fit of the points.

The results in this work compared to other current technologies for low threshold experiment are shown in Fig. 4(c). The plot was produced using the online tool provided by organizers of the EXCESS workshop [18]. Only data-sets from measurements above ground with published results are compared in the plot. Table I summarizes the references to the articles were the detector and data analysis information is presented. All spectra are normalized by efficiency. Our results do not show the rapidly increasing rate of events observed for the
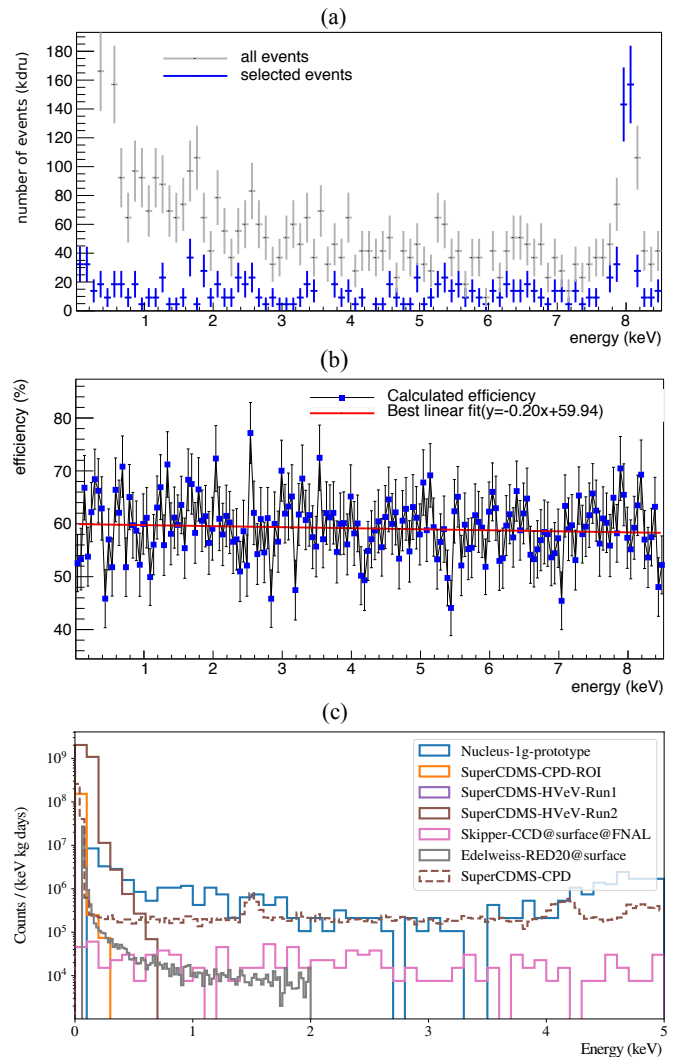

FIG. 4. (a) Energy spectrum before and after applying the selection criteria to the data (not weighted by the selection efficiency). The first two bins of the spectrum for all the events exceeds the selected maximum value in the $y - axes$. (b) efficiency of the selection cuts. (c) comparison of our results with other low energy technologies presented in [18].
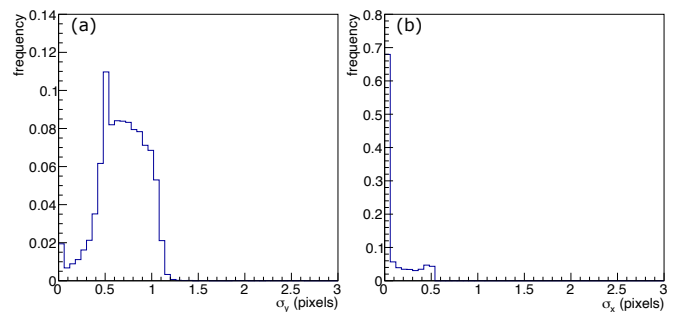

FIG. 5. Size distribution of events simulated in the active region of the sensor: (a) in the y-axis, (b) in the x-axis. The bins are normalized by the total number of simulated events.

other technologies for energies below 1 keV. Moreover, for energies below 500 eV where the neutrino signal from nuclear reactors is expected, our sensor shows the lowest background rate demonstrating the potential of the Skipper-CCD technology for this application and other low-energy measurements.

Legend in Figure 4(c)	References
Skipper-CCD@surface@FNAL	our results
Nucleus-1g-prototype	[28–32]
SuperCDMS-CPD-ROI	[33]
SuperCDMS-HVeV-Run1	[34]
SuperCDMS-HVeV-Run2	[35]
Edelweiss-RED20@surface	[36, 37]
SuperCDMS-CPD	[38]

TABLE I. References for the plots spectra shown in Fig. 4(c). References obtained from [18].

VI. CONCLUSIONS

Experimental results using a single-electron resolution Skipper-CCD running above ground have been presented. We demonstrated the potential of this technology for reactor neutrinos and other low-energy particle interaction experiments. The main background source of events has been identified and a technique to decouple its contribution has been presented. Our final result for events with energies of 5 ionized electron-hole pairs was compared to other state-of-the-art low-energy-threshold technologies showing that the exponentially increasing rate of events observed is not present in our data as shown in Fig. 4(c).

[1] A. Aguilar-Arevalo, D. Amidei, X. Bertou, M. Butner, G. Cancelo, A. Castañeda Vázquez, B. A. Cervantes Vergara, A. E. Chavarria, C. R. Chavez, J. R. T. de Mello Neto, et al. (DAMIC), *"Search for low-mass WIMPs in a 0.6 kg day exposure of the DAMIC experiment at SNO-LAB,"* Phys. Rev. **D94**, 082006 (2016), arXiv:1607.07410 [astro-ph.CO].

[2] A. Aguilar-Arevalo et al. (DAMIC), *"First Direct-Detection Constraints on eV-Scale Hidden-Photon Dark Matter with DAMIC at SNOLAB,"* Phys. Rev. Lett. **118**, 141803 (2017), arXiv:1611.03066 [astro-ph.CO].

[3] A. Aguilar-Arevalo et al. (DAMIC), *"Constraints on Light Dark Matter Particles Interacting with Electrons from DAMIC at SNOLAB,"* Phys. Rev. Lett. **123**, 181802 (2019), arXiv:1907.12628 [astro-ph.CO].

[4] M. Crisler, R. Essig, J. Estrada, G. Fernandez, J. Tiffenberg, M. Sofo haro, T. Volansky, and T.-T. Yu (SENSEI), *"SENSEI: First Direct-Detection Constraints on sub-GeV Dark Matter from a Surface Run,"* Phys. Rev. Lett. **121**, 061803 (2018), arXiv:1804.00088 [hep-ex].

[5] O. Abramoff et al. (SENSEI), *"SENSEI: Direct-Detection Constraints on Sub-GeV Dark Matter from a Shallow Underground Run Using a Prototype Skipper-CCD,"* Phys. Rev. Lett. **122**, 161801 (2019), arXiv:1901.10478 [hep-ex].

[6] G. Fernandez Moroni, J. Estrada, G. Cancelo, S. Holland, E. Paolini, and H. Diehl, *"Sub-electron readout noise in a skipper ccd fabricated on high resistivity silicon,"* Experimental Astronomy **34** (2012), 10.1007/s10686-012-9298-x.

[7] J. Tiffenberg, M. Sofo-Haro, A. Drlica-Wagner, R. Essig, Y. Guardincerri, S. Holland, T. Volansky, and T.-T. Yu, *"Single-electron and single-photon sensitivity with a silicon Skipper CCD,"* Phys. Rev. Lett. **119**, 131802 (2017), arXiv:1706.00028 [physics.ins-det].

[8] L. Barak, I. M. Bloch, M. Cababie, G. Cancelo, L. Chaplinsky, F. Chierchie, M. Crisler, A. Drlica-Wagner, R. Essig, J. Estrada, et al., *"SENSEI: Direct-Detection Results on sub-GeV Dark Matter from a New Skipper-CCD,"* arXiv e-prints , arXiv:2004.11378 (2020), arXiv:2004.11378 [astro-ph.CO].

[9] M. Settimo, *"Search for low-mass dark matter with the DAMIC experiment,"* arXiv e-prints , arXiv:2003.09497 (2020), arXiv:2003.09497 [hep-ex].

[10] The Oscura project is an R&D effort supported by Department of Energy to develop 10 kg skipper-CCD dark matter search.

[11] A. Aguilar-Arevalo, X. Bertou, C. Bonifazi, G. Cancelo, A. Castañeda, B. Cervantes Vergara, C. Chavez, J. C. D'Olivo, J. C. Dos Anjos, J. Estrada, et al. (CONNIE Collaboration), *"Exploring low-energy neutrino physics with the coherent neutrino nucleus interaction experiment,"* Phys. Rev. D **100**, 092005 (2019).

[12] CONNIE Collaboration, A. Aguilar-Arevalo, X. Bertou, C. Bonifazi, G. Cancelo, B. A. Cervantes-Vergara, C. Chavez, J. C. D'Olivo, J. C. Dos Anjos, J. Estrada, et al., *"Search for light mediators in the low-energy data of the CONNIE reactor neutrino experiment,"* Journal of High Energy Physics **2020**, 54 (2020), arXiv:1910.04951 [hep-ex].

[13] The Violeta Collaboration is planning a kg-scale Skipper-CCD experiment at a nuclear reactor facility.

[14] P. Du, D. Egana-Ugrinovic, R. Essig, and M. Sholapurkar, *"Sources of low-energy events in low-threshold dark matter detectors,"* (2020), arXiv:2011.13939 [hep-ph].

[15] G. F. Moroni, K. Andersson, A. Botti, J. Estrada, D. Rodrigues, and J. Tiffenberg, *"Charge-collection efficiency in back-illuminated charge-coupled devices,"* Phys. Rev. Applied **15**, 064026 (2021).

[16] A. Rubio-Montero, R. Pagán-Muñoz, R. Mayo-García, A. Pardo-Diaz, I. Sidelnik, and H. Asorey (LAGO), *"The EOSC-Synergy cloud services implementation for the Latin American Giant Observatory (LAGO),"* Proceedings, 37th International Cosmic Ray Conference (ICRC 2021) July 12th – 23rd, 2021, Online – Berlin, Germany, PoS **ICRC2021** (2021).

[17] R. Calderón-Ardila, A. Jaimes-Motta, J. Peña-Rodríguez, C. Sarmiento-Cano, M. Suárez-Durán, A. Vásquez-Ramírez, and for the LAGO Collaboration (LAGO), *"Modeling the LAGO's detectors response to secondary particles at ground level from the Antarctic to Mexico,"* Proceedings, 36th International Cosmic Ray Conference (ICRC 2019):Madison, WI, U.S.A., July 24-August 1, 2019, PoS **ICRC2019** (2019).

[18] E. Workshop, "Data repository," (2021).

[19] G. Fernandez-Moroni, P. A. N. Machado, I. Martinez-Soler, Y. F. Perez-Gonzalez, D. Rodrigues, and S. Rosauro-Alcaraz, *"The physics potential of a reactor neutrino experiment with Skipper CCDs: Measuring the weak mixing angle,"* JHEP **03**, 186 (2021), arXiv:2009.10741 [hep-ph].

[20] "Sunpower cyocoolers," .

[21] Https://engineering.lbl.gov/microsystems-laboratory/.

[22] G. I. Cancelo, C. Chavez, F. Chierchie, J. Estrada, G. Fernandez-Moroni, E. E. Paolini, M. S. Haro, A. Soto, L. Stefanazzi, J. Tiffenberg, et al., *"Low threshold acquisition controller for Skipper charge-coupled devices,"* Journal of Astronomical Telescopes, Instruments, and Systems **7**, 1 (2021).

[23] J. R. Janesick, *Scientific charge-coupled devices*, Vol. 83 (SPIE press, 2001).

[24] S. E. Holland, D. E. Groom, N. P. Palaio, R. J. Stover, and M. Wei, *"Fully depleted, back-illuminated charge-coupled devices fabricated on high-resistivity silicon,"* IEEE Transactions on Electron Devices **50**, 225 (2003).

[25] D. Rodrigues, K. Andersson, M. Cababie, A. Donadon, A. Botti, G. Cancelo, J. Estrada, G. Fernandez-Moroni, R. Piegaia, M. Senger, et al., *"Absolute measurement of the fano factor using a skipper-ccd,"* Nuclear Instruments and Methods in Physics Research Section A: Accelerators, Spectrometers, Detectors and Associated Equipment **1010**, 165511 (2021).

[26] L. Barak, I. M. Bloch, A. Botti, M. Cababie, G. Cancelo, L. Chaplinsky, F. Chierchie, M. Crisler, A. Drlica-Wagner, R. Essig, et al., "Sensei: Characterization of single-electron events using a skipper-ccd," (2021), arXiv:2106.08347 [physics.ins-det].

[27] M. S. Haro, G. Fernandez Moroni, and J. Tiffenberg, *"Studies on small charge packet transport in high-resistivity fully depleted ccds,"* IEEE Transactions on Electron Devices **67**, 1993 (2020).

[28] R. Strauss, J. Rothe, G. Angloher, A. Bento, A. Gütlein, D. Hauff, H. Kluck, M. Mancuso, L. Oberauer, F. Petricca, et al., *"Gram-scale cryogenic calorimeters for rare-event searches,"* Phys. Rev. D **96**, 022009 (2017).

[29] R. Strauss, J. Rothe, G. Angloher, A. Bento, A. Gütlein, D. Hauff, H. Kluck, M. Mancuso, L. Oberauer, F. Petricca, et al., *"Gram-scale cryogenic calorimeters for rare-event searches,"* Physical Review D **96** (2017), 10.1103/physrevd.96.022009.

[30] G. Angloher, P. Bauer, A. Bento, C. Bucci, L. Canonica, X. Defay, A. Erb, F. v. Feilitzsch, N. F. Iachellini, P. Gorla, et al., *"Results on mev-scale dark matter from a gram-scale cryogenic calorimeter operated above ground,"* The European Physical Journal C **77**, 637 (2017).

[31] B. Flebus, G. E. W. Bauer, R. A. Duine, and Y. Tserkovnyak, *"Theory of the magnon-mediated tunnel magneto-seebeck effect,"* Physical Review B **96** (2017), 10.1103/physrevb.96.094429.

[32] J. Rothe, G. Angloher, F. Ardellier-Desages, A. Bento, L. Canonica, A. Erhart, N. Ferreiro, M. Friedl, V. M. Ghete, D. Hauff, et al., *"Nucleus: Exploring coherent neutrino-nucleus scattering with cryogenic detectors,"* Journal of Low Temperature Physics **199**, 433 (2020).

[33] C. W. Fink, S. L. Watkins, T. Aramaki, P. L. Brink, J. Camilleri, X. Defay, S. Ganjam, Y. G. Kolomensky, R. Mahapatra, N. Mirabolfathi, et al., *"Performance of a large area photon detector for rare event search applications,"* Applied Physics Letters **118**, 022601 (2021).

[34] R. Agnese, T. Aralis, T. Aramaki, I. J. Arnquist, E. Azadbakht, W. Baker, S. Banik, D. Barker, D. A. Bauer, T. Binder, et al., *"First dark matter constraints from a supercdms single-charge sensitive detector,"* Phys. Rev. Lett. **121**, 051301 (2018).

[35] D. W. Amaral, T. Aralis, T. Aramaki, I. J. Arnquist, E. Azadbakht, S. Banik, D. Barker, C. Bathurst, D. A. Bauer, L. V. S. Bezerra, et al., *"Constraints on low-mass, relic dark matter candidates from a surface-operated supercdms single-charge sensitive detector,"* Phys. Rev. D **102**, 091101 (2020).

[36] E. Armengaud, C. Augier, A. Benoît, A. Benoit, L. Bergé, J. Billard, A. Broniatowski, P. Camus, A. Cazes, M. Chapellier, et al. (EDELWEISS Collaboration), *"Searching for low-mass dark matter particles with a massive ge bolometer operated above ground,"* Phys. Rev. D **99**, 082003 (2019).

[37] E. Armengaud, C. Augier, A. Benoît, A. Benoit, L. Bergé, J. Billard, A. Broniatowski, P. Camus, A. Cazes, M. Chapellier, et al., *"Searching for low-mass dark matter particles with a massive ge bolometer operated above ground,"* Physical Review D **99** (2019), 10.1103/physrevd.99.082003.

[38] I. Alkhatib, D. W. P. Amaral, T. Aralis, T. Aramaki, I. J. Arnquist, I. A. Langroudy, E. Azadbakht, S. Banik, D. Barker, C. Bathurst, et al., "Light dark matter search with a high-resolution athermal phonon detector operated above ground," (2021), arXiv:2007.14289 [hep-ex].